Electronic Supplementary Material (ESI) for ChemComm.
This journal is © The Royal Society of Chemistry 2023

Electronic Supplementary Material (ESI) for Chemical Communications.
This journal is © The Royal Society of Chemistry 2023

Supplementary Information

Phase-depended selectivity control over TiO_2 in the photocatalytic oxidation of bio-polyols

Fuao Jia, Hongru Zhou, Min Wang *

Affiliations:

School of Chemistry, Dalian University of Technology, Dalian 116024, Liaoning, China.

*Correspondence to: wangmin@dlut.edu.cn

Table of contents

Materials and Methods

Materials

All commercial chemicals were analytical reagents and were used without further purification. Glycerol, acetonitrile, and ethyl acetate were purchased from Tianjin Kermel Chemical Reagent Co. Ltd. Methyl formate, ethyl formate, benzyl formate, 2-phenethyl formate, methyl acetate, 2-phenethyl acetate, isopropyl titanate, anhydrous formic acid, dihydroxyacetone, KBr (SP) and xylose was purchased from Shanghai Macklin Biochemical Co., Ltd. Ethanol was purchased from Tianjin Damao Chemical Reagent Factory. Fructose was purchased from Sinopharm Chemical Reagent Co., Ltd. Glycolic acid and benzyl acetate was purchased from Aladdin Chemistry Co. Ltd. Other alditols and glyceraldehyde were purchased from Alfa Aesar. Water was purified using a Millipore Milli-Q Advantage A10 water purification system to a resistivity higher than 18 MΩ.cm. O_2 (>99.999%) and Ar (>99.999%) were provided by Dalian Junfeng Gas Chemicals Co. Ltd.

Catalyst preparation

Anatase TiO_2 was purchased from Shanghai Macklin Biochemical Co., Ltd. Rutile TiO_2 was synthesized via a hydrothermal method with titanium isopropoxide as the Ti source. Typically, 10 mL of deionized water and 10 mL of 38% hydrochloric acid were added to 10 mL of titanium isopropoxide. Then the mixture was transformed into a 50 mL Teflon-lined autoclave and was maintained at 180 °C for 24 h. After the autoclave naturally cooled down to room temperature, the white precipitate was washed with 1M NaOH, ethanol, and deionized water until the pH at 7 and dried in an electric oven at 60 °C. Finally, the white powder was calcined at 500 °C in a muffle furnace for 3 h with a temperature rate of 5 °C min^{-1} to remove the organics of the catalyst. [1]

Catalyst performance evaluation

Reaction and testing of photocatalytic activity were carried out in homemade LED photoreactors. For the standard reaction conditions, 10 mg of the glycerol and 5 mg of catalyst were mixed in 1 mL of solvent (0.95 mL of acetonitrile and 0.05 mL of H_2O), then the system was completely

replaced with O_2 before being sealed with a cap. After that, the quartz tube was stirred for some time in the darkness and then irradiated with 365 nm LED light (18 W, 55 mW cm^{-2}) via side irradiation. After the reaction, 100 μL of He was injected into the gas-phase products as the inner standard. The gas-phase products were quantified by gas chromatography (GC, TianMei) equipped with a TCD detector and TDX-01 column. A 500 μL of reacted gas was injected into the GC via an injector. The catalyst was filtered, and the supernatant was analyzed by the GC-MS (Agilent) equipped HP-5 column, and high-performance liquid chromatography (HPLC, Shimadzu, LC-2030 Plus, Japan) equipped with a hydrogen column (ROA-Organic Acid H+ (8%), 300 × 7.8 mm).

Supplementary Methods

Characterization

X-ray diffraction (XRD) patterns of the prepared catalysts were conducted with a Smartlab 9 kW (Rigaku Corporation) diffractometer, using Cu-Kα radiation at 45 kV and 200 mA. The 2 theta range was scanned from 10° to 80°. UV-vis diffuse reflectance spectra (UV-vis DRS) were recorded on a UV-vis spectrophotometer (Agilent UV-550) at room temperature in the range of 200-800 nm with BaSO4 as the background. X-ray photoelectron spectroscopy (XPS) analysis was obtained by ESCALAB250Xi (Thermo, USA) using Al Kα (hv=1486.6 eV) as the exciting source. The binding energies of Ti 2p, O 1s were corrected by C 1s (284.8 eV). BET surface analysis, the surface area of the TiO_2 nanoparticles was examined with the nitrogen (N_2) adsorption-desorption. investigation.

In-situ Fourier transform infrared (FTIR)

In-situ FTIR spectroscopy was carried out on Nicolet iS 10 IR spectrometer equipped with the MCT/A detector. Typically, 5 mg of TiO_2 and 50 mg of KBr (SP) were mixed and ground to a uniform powder. Then the mixture was pressed into a thin sheet and placed into the reaction cell. Before the test, a background spectrum was recorded using 32 scans and then subtracted automatically from the subsequent spectra. After that, 50 μL of anhydrous formic acid was dripped into the thin sheet. After dried 3 min, the thin sheet was irradiated by a 300 W Xe lamp and the FTIR spectra started recording.

Pyridine adsorption Infrared (Py-IR)

Pyridine adsorption Infrared (Py-IR) spectra were collected by using a Bruker TENSOR 27 IR spectrometer. The resolution of the instrument is $4cm^{-1}$, and the number of scan accumulations is 32. Weigh 40 mg of the catalyst and press it into a uniform sheet, and place the sample sheet in a 50ml/min N_2 gas stream to heat 200℃ for pretreatment. The temperature is then lowered to 150℃, at which temperature the sample background is collected. After that, the sample was cooled to 25℃, and pyridine was adsorbed on it for 30 minutes, and then the temperature was raised to 150℃ to measure its pyridine adsorption infrared spectrum.

Products analysis

The gas products were quantified via the internal standard method by a Tianmei gas chromatograph (GC) equipped with a TCD detector and TDX-01 column. The O_2 contents during the photoreaction were quantified via the internal standard method by a Tianmei gas chromatograph (GC) equipped with a TCD detector and 13 X column (3 m × 2mm). He was used as the internal standard. The GC peak area was used for calculation. The differential response was calibrated using the response factor. The detailed calculation was as follows:

$$V_{CO} = A_{CO}/A_{He} \times V_{He} \times K_{CO}$$

$$V_{CH_4} = A_{CH_4}/A_{He} \times V_{He} \times K_{CH_4}$$

$$V_{CO_2} = A_{CO_2}/A_{He} \times V_{He} \times K_{CO_2}$$

In these equations:

V_{CO}: the volume of produced CO; V_{CH_4}: the volume of produced CH_4; V_{CO_2}: the volume of produced CO_2; V_{He}: the He volume injected in the reactor; A_{CO}: the peak area of CO in GC; A_{CH_4}: the peak area of CH_4 in GC; A_{CO_2}: the peak area of CO_2 in GC; A_{He}: the peak area of He in GC; K_{CO}: the CO response factor related to He in Tianmei GC; K_{CH_4}: the CH_4 response factor related to He in Tianmei GC; K_{CO_2}: the CO_2 response factor related to He in Tianmei GC.

The produced FA was quantified by a high-performance liquid chromatography (HPLC, Shimadzu, LC-2030 Plus, Japan) equipped with a hydrogen column (ROA-Organic Acid H+ (8%), 300 × 7.8 mm) and a UV and RID detector *via* external standard method. The detailed calculation was as follows:

$$m_{FA} = A_{FA} \times K_{FA} \times V_{solvent}$$

In these equations:

m_{FA}: the mass of produced FA; A_{FA}: the peak area of FA in the UV detector of HPLC; K_{FA}: the CH_4 response factor UV detector of HPLC;

The yields of products are calculated based on the sum of total carbon in products and were as follows:

$$Y_P = (N_P \times C_P) / (N_{substrates} \times C_{substrates}) \times 100$$

Where Y_p is the yield of products; N_p is the calculated mole number of products; C_p is the carbon number in products; $N_{substrates}$ is the molar of substrates; $C_{substrates}$ is the carbon number in substrates.

Where the S_{CO} is the selectivity of CO in gas products; N_{CO} is the calculated mole number of CO; N_{CH_4} is the calculated mole number of CH_4; N_{CO_2} is the calculated mole number of CO_2.

The molar of gas products is calculated based on the gas equation.

$$N_G = V_G / 22.4$$

Where the N_G is the molar of gas products; V_G is the calculated volume of gas products by GC.

DFT calculation

The DFT calculation was carried out using the Vienna ab initio simulation package (VASP).[2] The exchange-correlation potential was described by the Perdew-Burke-Ernzerhof (PBE)[3] formulation of the generalized gradient approximation (GGA). The interactions between ionic cores and valence electrons were described by the projected augmented wave (PAW) [4] method. A plane wave basis set with an energy cutoff of 400 eV was used and the *k*-point sampling was performed using the Monkhorst-Pack scheme.[5] The electronic self-consistent minimization converged to 10^{-5} eV, and the geometry optimization converged to -0.02 eV $Å^{-1}$. The lattice constants of anatase TiO_2-A were optimized to be a = 3.802 Å, b = 3.802 Å, and c = 9.486 Å. The lattice constants of rutile TiO_2-R were optimized to be a = b = 4.60657 Å, c = 2.95900 Å. We used them to build a (2 × 2) TiO_2-A and TiO_2-R slab with a vacuum of 15 Å. Atoms in the bottom 2 atomic layers were fixed to their bulk positions, while the rest were allowed to fully relax. A 4 × 2 × 1 and 4 × 4 × 1 *k*-point mesh was used for TiO_2-A and TiO_2-R slab, respectively. The combination of nudged elastic band (NEB) method[6] and the dimer method[7] was used to search the transition state. The spin density of photogenerated electrons was calculated by adding electrons into the supercell according to the literature.[8, 9]

Supplementary Figures

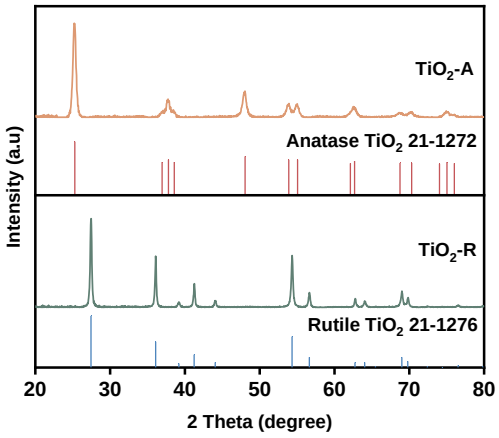

Fig. S1 | Catalyst characterization. XRD patterns of the TiO_2-A and TiO_2-R.

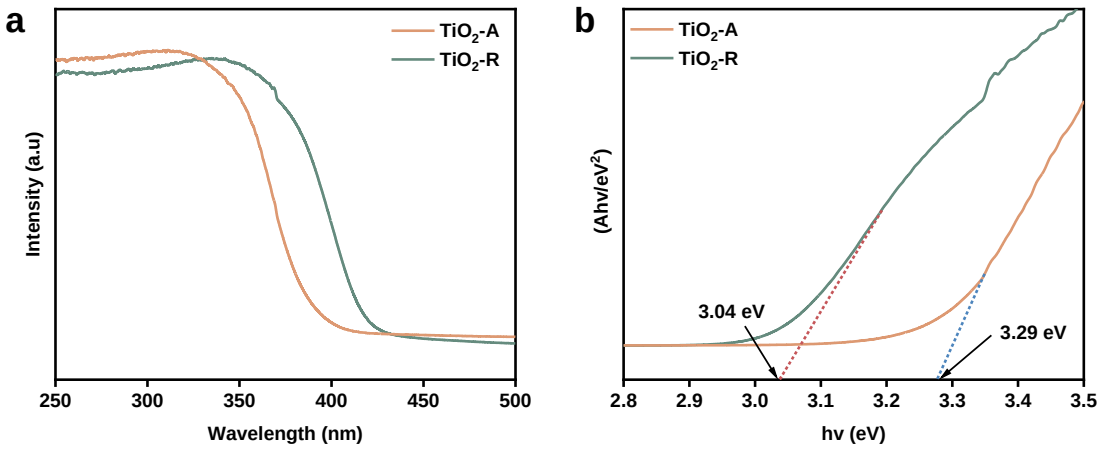

Fig. S2 | Catalyst characterization. DRS spectra of TiO_2-A and TiO_2-R.

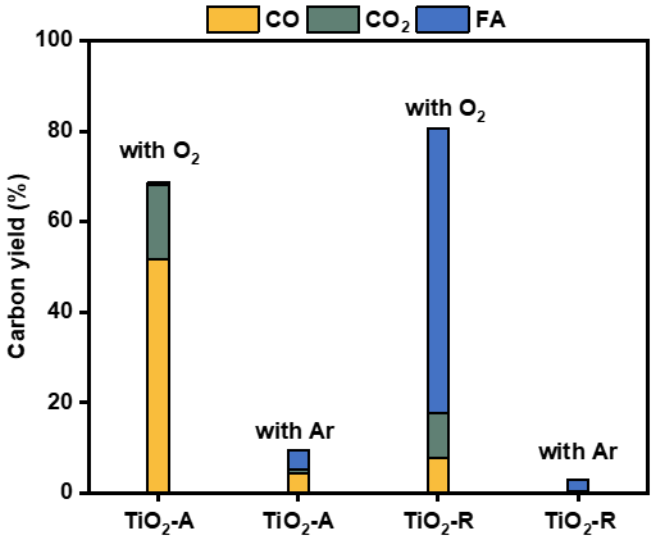

Fig. S3 | Photocatalytic conversion of glycerol under Ar and O_2. Reaction conditions: 5 mg of TiO_2, 10 mg of glycerol, 0.95 mL of MeCN, 0.05 mL of H_2O, 365 nm LED, 24 h.

The role of O_2 has been clarified in our previous work[10, 11]. The addition of O_2 can improve the thermodynamic process of biomass reforming reaction thus reducing the reaction energy barrier. O_2 can be reduced by photogenerated electrons and produce superoxide and hydroxyl radicals thus accelerating the oxidative reaction. We also compared the glycerol reforming activity over TiO_2 under Ar and O_2 atmospheres. In an inert atmosphere, TiO_2 also possesses the ability to reform glycerol into CO or FA but with low activity The introduction of O_2 significantly increases the reaction rate of glycerol reforming.

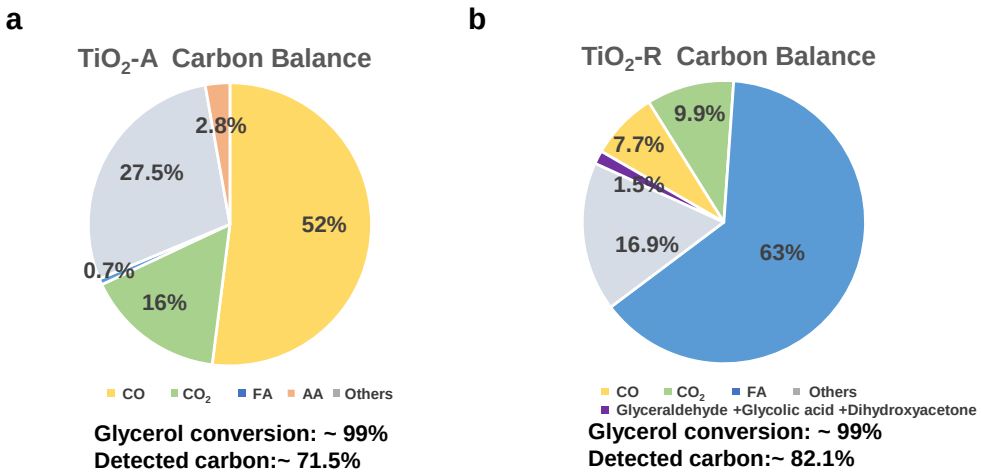

Fig. S4 | Carbon balance data during glycerol reforming over TiO_2. Reaction conditions: 5 mg of TiO_2, 10 mg of glycerol, 0.95 mL of MeCN, 0.05 mL of H_2O, 365 nm LED, O_2, 24 h.

The glycerol conversion rate on both TiO_2 surfaces has reached over 99% and the carbon balance is 71.5% and 82.1% over TiO_2-A and TiO_2-R, respectively. Previous literature has reported that TiO_2 can catalyze the alcohol coupling reaction during photocatalysis[1], which might result in the production of big molecules and cannot be detected by HPLC. Besides, some carbon-containing molecules are adsorbed on the surface of the catalyst, which can also cause some carbon loss.

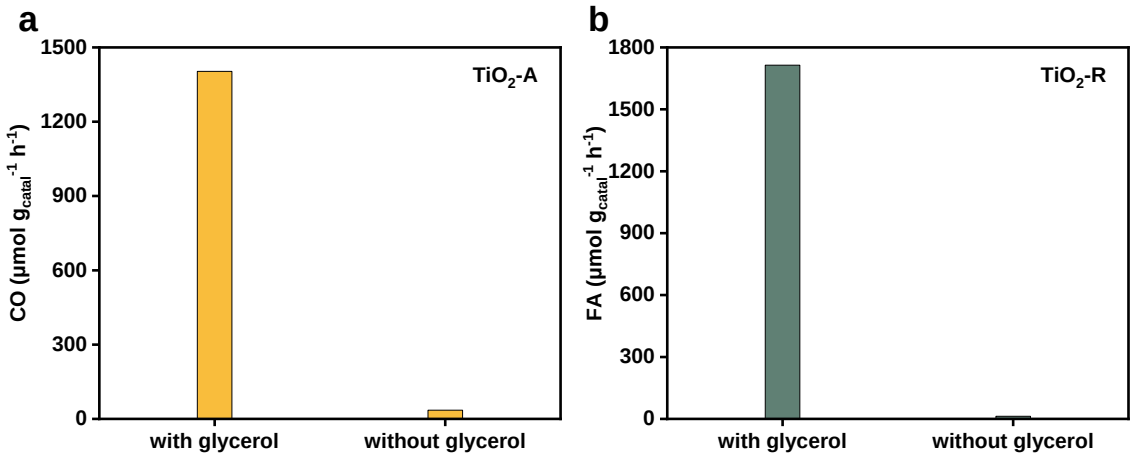

Fig. S5 | Blank experiment. a, CO production over TiO_2-A. **b**, FA production over TiO_2-R. Reaction conditions: 10 mg of glycerol, 5 mg of catalysts, 950 μL of acetonitrile, 50 μL of H_2O, 365 nm LEDs, 24 h.

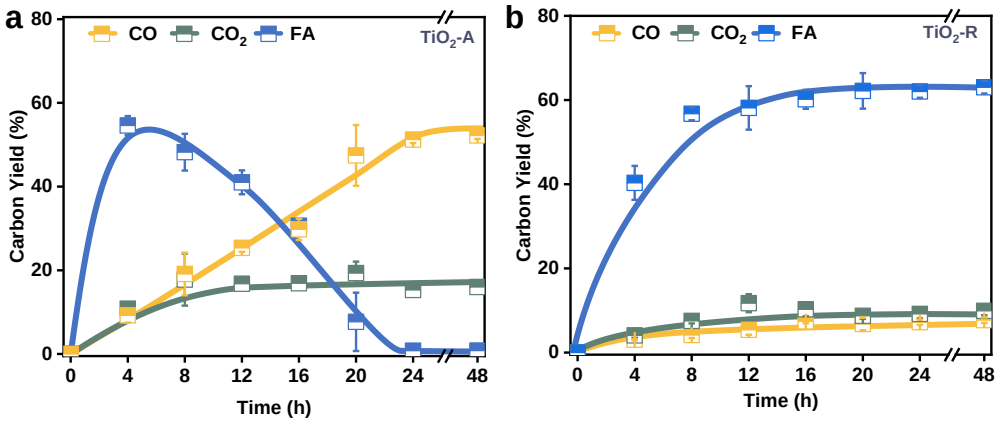

Fig. S6 | Photocatalytic conversion of glycerol. Reaction conditions: 5 mg of TiO_2, 10 mg of glycerol, 0.95 mL of MeCN, 0.05 mL of H_2O, 365 nm LED, O_2.

Firstly, we have extended the response time to 48 hours. The results demonstrated that the produced CO over TiO_2-A, and FA is stable over TiO_2-A. Besides, we subsequently conducted three parallel experiments repeatedly, and the results showed that the same product profiles can be achieved using the same catalyst. All these experiments confirm that the product profiles in subsequent reactions using the same catalyst are the same. The photocatalytic oxidation is conducted in the presence of O_2. The photogenerated election is dominantly used to reduce dioxygen. Only a minor amount of H_2 was generated as the reductive product.

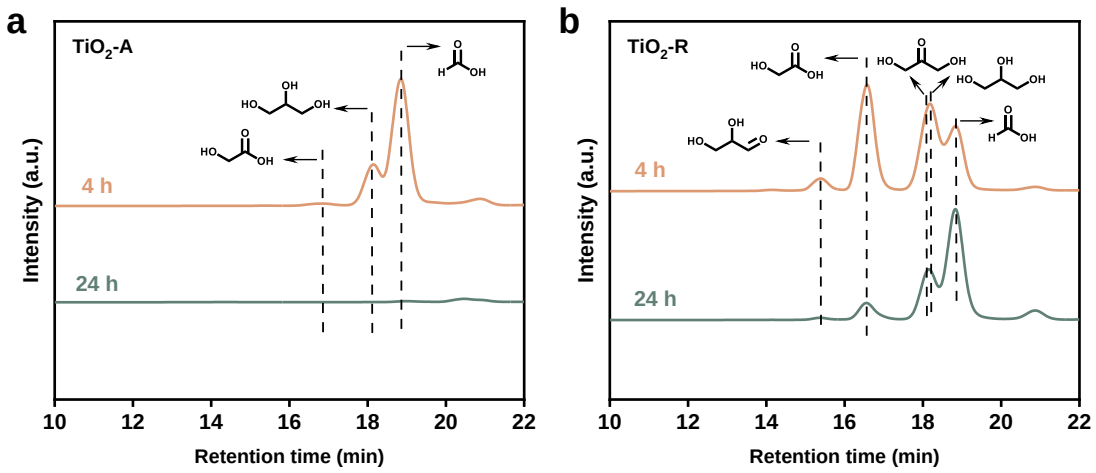

Fig. S7 | HPLC RID detector results of glycerol reforming over TiO_2. a, TiO_2-A. **b**, TiO_2-B. Reaction conditions: 10 mg of glycerol, 5 mg of catalysts, 950 μL of acetonitrile, 50 μL of H_2O, 1 atm of O_2, 365 nm LEDs.

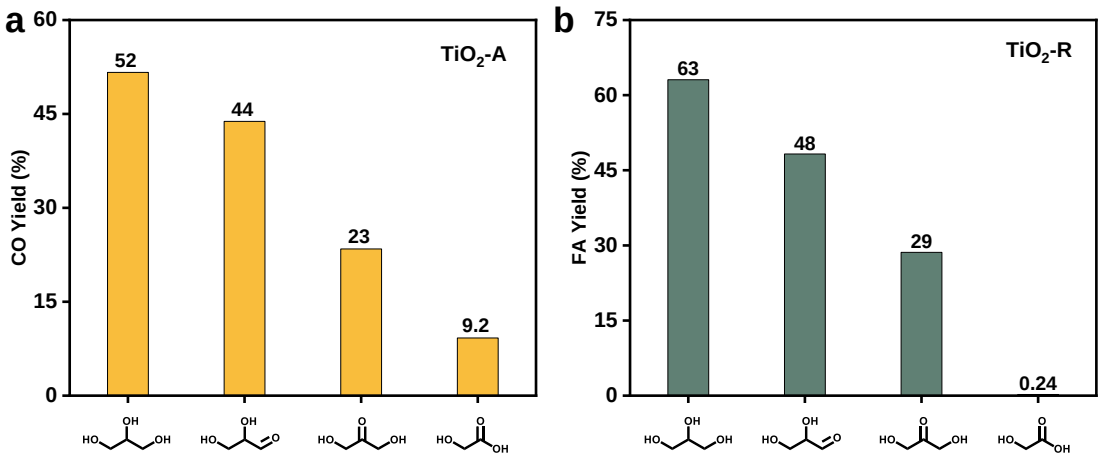

Fig. S8 | CO and FA production from photo-reforming of different glycerol oxidation intermediate over TiO_2-A and TiO_2-R. Reaction conditions: 5 mg of catalysts, 0.1 mmol of substrates, 950 μL of acetonitrile, 50 μL of H_2O, 365 nm LEDs, 1 atm of O_2, 24 h.

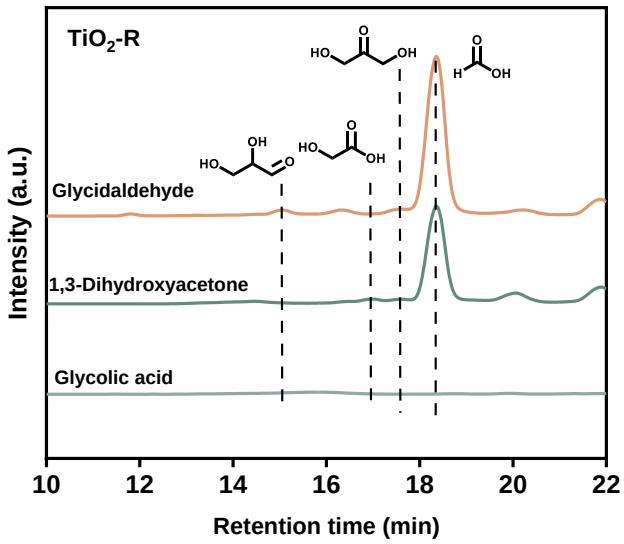

Fig. S9 | HPLC RID detector results of different intermediates reforming over TiO_2-R. Reaction conditions: 5 mg of catalysts, 0.1 mmol of substrates, 950 μL of acetonitrile, 50 μL of H_2O, 365 nm LEDs, 1 atm of O_2, 24 h.

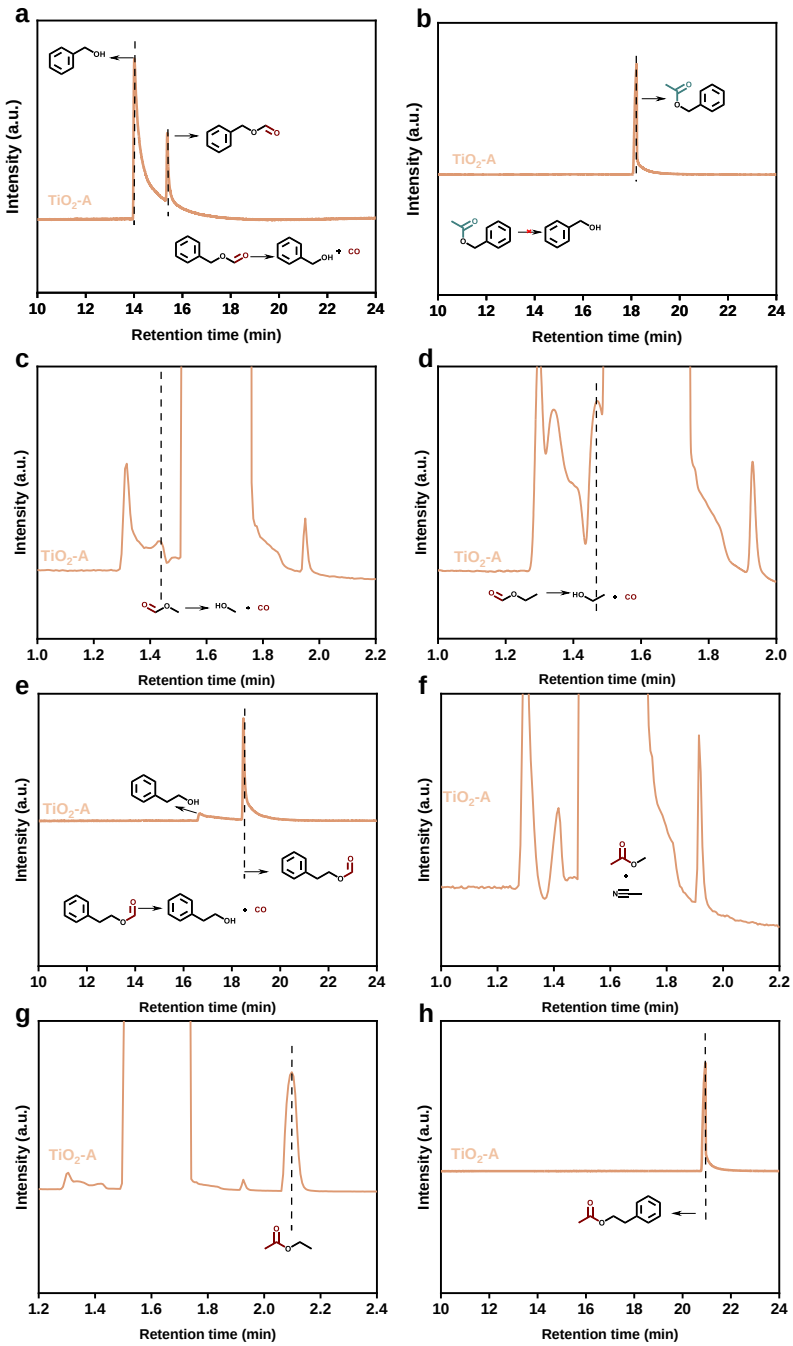

Fig. S10 | GC-MS spectra of photocatalytic esters decomposition over TiO_2-A. a, benzyl formate. **b,** benzyl acetate. **c**, methyl formate. **d,** ethyl formate. **e,** phenethyl formate. **f,** methyl acetate. **g,** ethyl acetate. **h,** phenylethyl acetate. Reaction conditions: 5 mg of catalyst, 0.22 M of substrates, 1 mL of acetonitrile, 1 atm of Ar, 365 nm LED, 24 h.

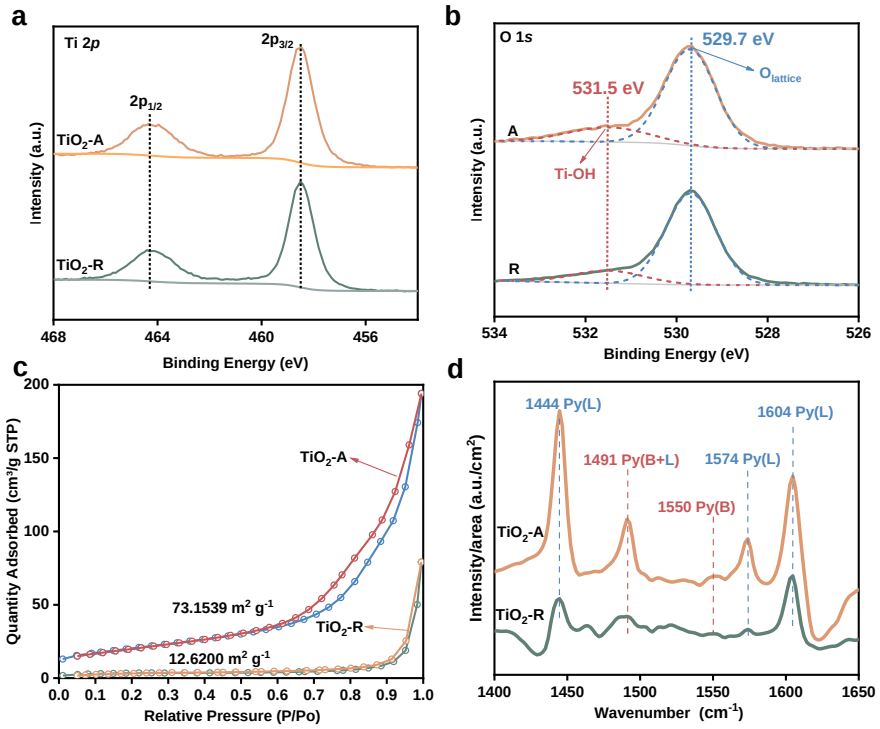

Fig. S11 | Basic characterization of TiO_2-A and TiO_2-R. (a-b) Ti 2p and O1s XPS spectra, (c) BET spectra, (d) Pyridine-adsorption FTIR.

To exclude other effects on FA dehydration activity, we characterized the surface properties of the two TiO_2 samples (Fig. S11). XPS analysis revealed that both TiO_2 samples possess similar surface chemical environments (Fig. S4a, b). N_2 adsorption-desorption experiments indicated that both TiO_2-A and TiO_2-R have similar pore structures, although TiO_2-A exhibits a higher specific surface area (Fig. S4c). we conducted additional experiments using pure formic acid as the substrate. Remarkably, when pure formic acid was used, TiO_2-A displayed nearly complete conversion with an 84% yield of CO, while TiO_2-R exhibited almost no activity (manuscript Fig. 2b). This result indicates that the discrepancy in selectivity between the two TiO_2 samples is not primarily attributed to their specific surface areas.

Further analysis using pyridine-adsorbed FTIR spectra demonstrated that both TiO_2 samples contain acid sites[12, 13], despite the content of these sites differs (Fig. S4d).

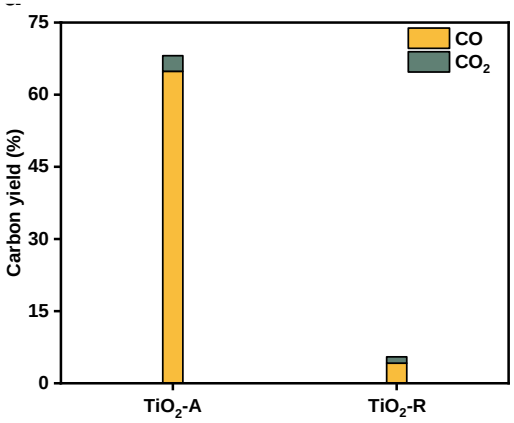

Fig. S12 | Influences of pyridine on the catalytic activity of TiO_2-A/R for formic acid dehydration. Reaction conditions: 5 mg of TiO_2, 10 mg of FA, 1 mL of MeCN, 0.2 mL Pyridine,365 nm LED, Ar).

To explore the possibility that acid sites could be the major cause for the disparity in FA dehydration activity between the two TiO_2 samples, we performed additional experiments by introducing pyridine to block the acid sites. Even after blocking the acid sites, TiO_2-A remained significantly more active than TiO_2-R in the decomposition of formic acid (Fig. S12). These findings indicate that the differences in surface defects and acidic sites are not the predominant factors influencing the variation in FA dehydration activity between the two TiO_2 samples.

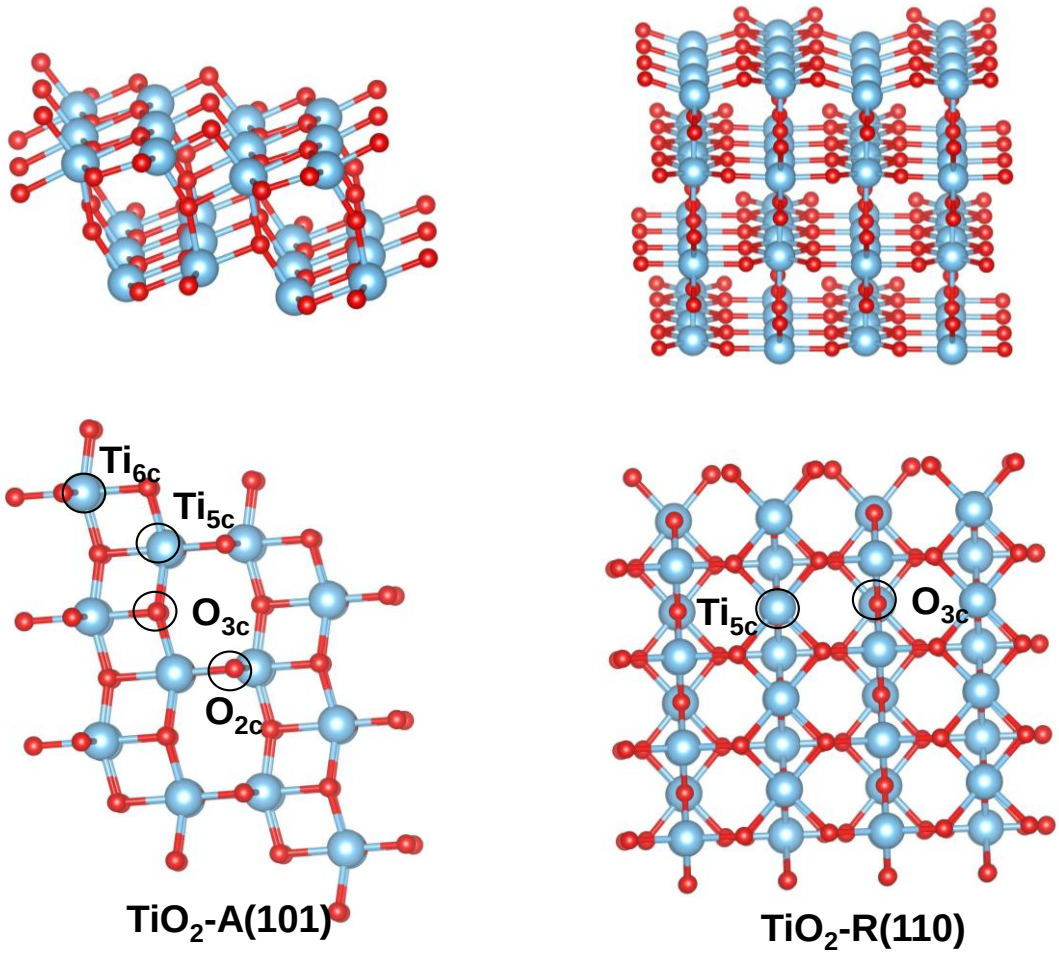

Fig. S13 | The surface geometry of TiO_2-A(101) and TiO_2-R(110)

After excluding some effects, we think it is the natural surface geometry that affects the observed different FA adsorption configurations. Anatase and rutile show different surface geometry and the surface coordination state and the alignment of the surface atom are different for the most stable TiO_2-A(101) and TiO_2-R(110) surfaces. As shown below, the anatase surface contains five coordinated Ti_{5c}, six coordinated Ti_{6c}, two coordinated $O_{2c,}$ and three coordinated O_{3c}, while rutile only contains Ti_{5c} and O_{3c}. Moreover, the alignment of the surface atom is also very different. These surface characteristics affect the adsorption configuration of FA. As shown by DFT calculation (manuscript Fig. 3), monodentate molecular adsorption (HCOOH-mono) adsorption with the oxygen in the carbonyl group is coordinated to Ti_{5c} and the H in -OH group interacting with O_{2c} via hydrogen-bonding is the most stable adsorption mode. While for TiO_2-R, the mostly stable adsorption mode is the bidentate dissociated adsorption (HCOO-bi) adsorption with two oxygen coordinated with two neighborly Ti_{5c}. This different FA adsorption configuration accounts for the FA dehydration.

Reference

1. X. J. Wu, J. Q. Li, S. J. Xie, P. B. Duan, H. K. Zhang, J. Feng, Q. H. Zhang, J. Cheng and Y. Wang, *Chem*, 2020, **6**, 3038-3053.
2. G. Kresse and J. Furthmuller, *Comput. Mater. Sci.*, 1996, **6**, 15-50.
3. J. P. Perdew, K. Burke and M. Ernzerhof, *Phys. Rev. Lett.*, 1996, **77**, 3865-3868.
4. G. Kresse and D. Joubert, *Phys. Rev. B.*, 1999, **59**, 1758-1775.
5. H. J. Monkhorst and J. D. Pack, *Phys. Rev. B*, 1976, **13**, 5188-5192.
6. G. Henkelman, B. P. Uberuaga and H. Jonsson, *J. Chem. Phys.*, 2000, **113**, 9901-9904.
7. G. Henkelman and H. Jonsson, *J. Chem. Phys.*, 1999, **111**, 7010-7022.
8. B. J. Morgan and G. W. Watson, *Phys. Rev. B*, 2009, **80**, 233102.
9. X. C. Ma, Y. Dai, M. Guo and B. B. Huang, *Langmuir*, 2013, **29**, 13647-13654.
10. H. R. Zhou, M. Wang and F. Wang, *Chem*, 2022, **8**, 465-479.
11. Z. Zhang, M. Wang and F. Wang, *Chem. Catal.*, 2022, **2**, 1394-1406.
12. W. J. Ni, D. J. Yan, S. J. Fu, Y. A. Wei, H. Y. Yang, X. W. Zhang, F. F. Zhao, K. Y. You and H. A. Luo, *Chem. Eng. J.*, 2023, **465**, 142905.
13. R. F. Chong, J. Li, Y. Ma, B. Zhang, H. X. Han and C. Li, *J. Catal.*, 2014, **314**, 101-108.